6-1980

A Comparison of the Solvent and Temperature Dependence of the Fluorescence Quantum Yield of Methyl-1-, Methyl-2-, and Methyl-9-Anthroate

David B. Lyon
Union College - Schenectady, NY

A COMPARISON OF THE SOLVENT AND TEMPERATURE DEPENDENCE OF
THE FLUORESCENCE QUANTUM YIELD OF METHYL-1-, METHYL-2-, AND
METHYL-9-ANTHROATE

by

David B. Lyon
///

* * * * * * *

Submitted in partial fulfillment
of the requirements for
Honors in the Department of Chemistry

UNION COLLEGE

March, 1980

ABSTRACT

LYON, DAVID A Comparison of the Solvent and Temperature
Dependence of the Fluorescence Quantum Yield of
Methyl-1-, Methyl-2-, and Methyl-9-Anthroate.
Department of Chemistry, March 1980

Two fluorescence parameters, the room temperature quan-
tum yield and the activation energy for nonradiative decay,
were studied for the three possible monosubstituted methyl
esters of anthroic acid in a number of aprotic, nonaromatic
solvents. For the 1 and 2 substituted esters, the quantum
yield increased and went through a maximum with decreasing
S_1 energy. In contrast, for methyl-9-anthroate, a general
monotonic decrease in quantum yield with decreasing S_1 energy
was found. We assume, that intersystem crossing is the only
nonradiative decay process that competes with fluorescence
for the esters. Since we find that the esters show temper-
ature dependent fluorescence, intersystem crossing must oc-
cur by thermal activation to a triplet energy level (T_x) that
lies higher in energy than the first singlet excited state
(S_1). An increase in solvent polarity lowers the S_1 energy
and has little effect on the relative position of T_x. Using
this model, we expect the lowering of the S_1 energy by sol-
vent to enhance the quantum yield for a given ester since
the S_1-T_x energy gap increases and therefore intersystem
crossing competes less effectively with fluorescence. The
activation energy is a measure of the S_1-T_x gap and is de-
termined by fitting the temperature dependence of the quan-

tum yield to an Arrhenius expression. Our results indicate
this simple model holds quite well for the 1 and 2 methyl-
anthroates, but that some other factor besides the $S_1 - T_x$
energy gap alone determines the nonradiative decay rate in
methyl-9-anthroate.

TABLE OF CONTENTS

INDEX OF FIGURES AND TABLES

I. Figures

II. Tables

INTRODUCTION

INTRODUCTION

Many aromatic molecules undergo electronic transitions when light of the ultraviolet and visible region of the electromagnetic spectrum impinges on them. Normally, a molecule resides in its lowest or ground electronic state, but when irradiated by light possessing energy corresponding to the difference in its electronic energy levels, molecules may absorb a photon and be excited to higher energy states. A molecular energy state diagram, or Jablonski diagram (Figure 1), for a typical molecule allows us to pictorially represent the transitions that may occur in the molecule.

In Figure 1, we see our ground state (S_0) molecule absorbing (A) energy and being excited to a higher energy state. Following absorption, the molecule resides in one of the many vibrational levels of the excited state, here being S_2. The molecule rapidly loses its excess vibrational energy by vibrational relaxation and ends up in the 0th vibrational level of S_1. From here, the molecule may return to its ground state by one of three processes: fluorescence (F), internal conversion (IC), intersystem crossing (ISC).

Fluorescence is the radiative deactivation of S_1 to some vibrational level of S_0. The energy of the photon emitted during fluorescence is equal to the energy difference

Figure 1

Jablonski Diagram

Following absorption of light (A), a molecule under-
goes rapid electronic and/or vibrational relaxation to the
lowest vibrational level of S_1. Deactivation of S_1 to S_C
may occur by either fluorescence (F), a radiative process,
or by internal conversion (IC), a nonradiative process.
Intersystem crossing (ISC) is a nonradiative process which
results in the formation of a triplet state from which either
phosphorescence (P) or reverse intersystem crossing may
return the molecule to the ground state.
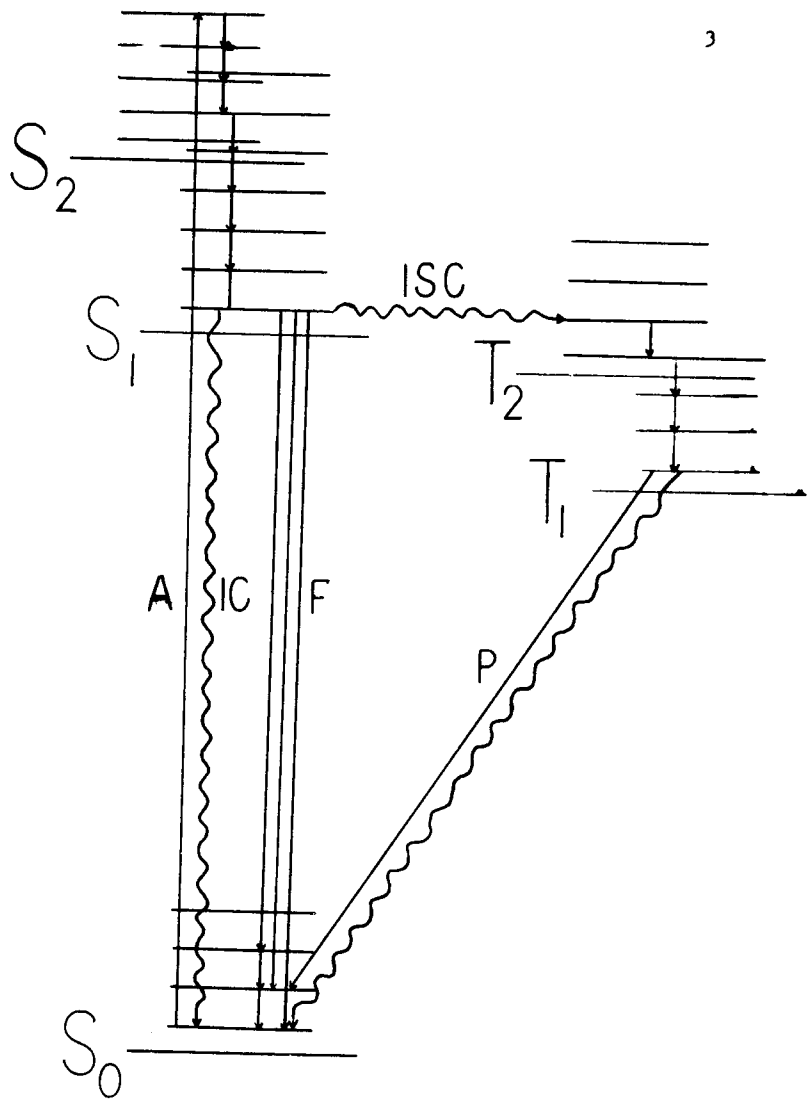
between the lowest vibrational level of S_1 and the vibrational level of S_0 at which the transition terminates. Vibrational structure observed in the emission spectra of some molecules is due to the fact that the fluorescence transition can terminate in one of several vibrational levels of S_0. Once in a vibrational level of S_0, rapid vibrational relaxation occurs to the 0th vibrational level.

The two processes that compete with fluorescence in deactivating S_1, internal conversion and intersystem crossing are both nonradiative mechanisms. Internal conversion occurs between S_1 and S_0 by vibrational relaxation in which the excess electronic energy is released to the solvent environment as thermal energy. Intersystem crossing is a transition which results in the formation of a triplet state, characterized by having two electrons with unpaired spins. Intersystem crossing occurs when one of the vibrational levels of S_1 is isoenergetic with a vibrational level of a nearby triplet (T_2 in Figure 1). Although intersystem crossing is quantum mechanically forbidden because of the change in spin quantum number, spin-orbit coupling introduces triplet character into the singlet state and visa versa. The resultant state mixing makes the S_1-T_x transition probability nonzero. Upon entering the triplet manifold, vibrational and electronic relaxation leave the molecule in the 0th virational level of T_1. The return to S_0 occurs

either by the radiative process phosphorescence (P), or by radiationless reverse intersystem crossing, T_1-S_0.

The number of photons emitted via fluorescence divided by the total number of photons absorbed defines the fluorescence quantum yield (ϕ_f). The quantum yield may be expressed in terms of the rate constants for the three processes that deactivate S_1: k_f, k_{ic}, k_{isc}. At any temperature, ϕ_f is equal to the ratio of the fluorescence rate constant to the sum of all rate constants for processes which depopulate S_1 (equation 1).

$$\phi_f(T)=k_f(T)/k_f(T)+k_{ic}(T)+k_{isc}(T) \tag{1}$$

Measurements of the lifetime of the excited state can be obtained by using a nanosecond flash to populate S_1 and recording the fluorescence decay as S_1 is deactivated. The time required for the fluorescence intensity to fall to 1/e of its initial value is the fluorescence lifetime (τ_f). Equation 2 expresses the fluorescence lifetime in terms of the processes deactivating S_1. The expression for τ_f is

$$\tau_f=1/k_f+k_{ic}+k_{isc} \tag{2}$$

valid at any temperature and thus equation 2 can be combined with equation 1 to give equation 3, an alternate expression for the fluorescence quantum yield.

$$\phi_f=k_f\tau_f \tag{3}$$

In this study, the three possible monosubstituted methyl esters of anthroic acid are the molecules of interest.

For monosubstitution of anthracene, the electron density at the 1 position is intermediate between the two other possible positions, 2 and 9. Molecular models of methyl-1-anthroate (1-COOME) demonstrate that the substituent cannot achieve complete coplanarity with the ring in the ground state due to interactions with neighboring hydrogens. X-ray analysis of 1-naphthoic acid places the angle between the carboxyl group and the parent ring at 11°.[1] Therefore, we expect a similar S_0 geometry for 1-COOME. Simple HMO calculations by Werner to determine the π bond order of the ring to carboxyl group bond in both the ground and first excited singlet states have shown that the π bond order is greater in S_1 than in S_0.[2] This suggests that the Franck-Condon equilibrium state from which fluorescence originates is characteristic of a molecular geometry in which the ring and carboxyl group are more nearly coplanar. In addition, it is known that carboxyl substitution introduces some charge transfer into the molecule resulting in a more polar excited state. Evidence for the charge transfer character of S_1 comes from findings by Werner that the carboxyl group becomes more basic on excitation.[3]

For substitution at the 2 position, the least electron-rich position, molecular models indicate no steric hindrance to coplanarity between the ring and carboxyl group. McGlynn and Lui have presented spectral evidence which shows methyl

and ethyl esters of 2-naphthoic acid are planar in the ground state which we extend to the S_0 geometry of methyl-2-anthroate.[4] HMO calculations also show a greater π bond order for S_1 than S_0 in 2-COOME.[2] The equilibrium state from which fluorescence originates is therefore characteristic of a coplanar molecular geometry. Due to a lower electron density at the 2 position, charge transfer is not as great as in 1-COOME and S_1 is not as polar for 2-COOME.

In the 9 or meso position, a substituent encounters the most electron-rich position of the parent anthracene ring and the substituent also lies along the polarization axis of the lowest anthracene electronic transition ($^1A_1$-^1L_a) responsible for the long wavelength absorption and fluorescen spectra of all three methyl-anthroates. Complete planarity between a substituent at the 9 position and the ring is prevented by steric interactions with the peri hydrogens (positions 1 and 8). The absorption spectrum of methyl-9-anthroate resembles that of anthracene, in agreement with the near perpendicularity of the ring and carboxyl group in S_0.[5] However, HMO calculations show the π bond order is greater in S_1 than in S_0.[2] On excitation, the significant increase in π bond order results from an S_1 geometry approaching coplanarity. Charge transfer toward the carboxyl group accompanies this geometry change. Thus, while 1-COOME undergoes a slight geometry change and 2-COOME

undergoes no geometry change, 9-COOME undergoes a substantial geometry change upon excitation to S_1.

Let us now turn our attention to the specific system of this study. The work was originated in an attempt to rationalize the solvent dependence of the fluorescence quantum yield of methyl-9- and methyl-2-anthroate.[6,7] In this study, some of the work of Hawkins and Facci was repeated using an upgraded experimental procedure for quantum yield versus temperature determinations. In addition, the third possible monosubstituted methyl ester of anthroic acid, methyl-1-anthroate, was included to compare its quantum yield dependence on solvent with the 9 and 2 substituted esters. In choosing solvents, we initially restricted ourselves to aprotic, nonaromatic solvents. Later, to increase the range of quantum yields for 9-COOME, we relaxed our restrictions to include two protic, nonaromatic solvents for this ester. Facci has shown specific hydrogen bonding and aromatic solvent effects on the fluorescence properties of methyl-anthroates which we wished to avoid as much as possible.[7]

EXPERIMENTAL

EXPERIMENTAL

Chemicals: Methyl-1-anthroate, methyl-2-anthroate, and methyl-9-anthroate were prepared by Werner and Matthews. (8,9) Purity checks were run on the esters in the following ways:

1) Melting point determinations
2) Recording fluorescence spectra in dilute ethanol

The appearance of superimposed fine structure in the fluorescence spectra in dilute ethanol would indicate the presence of either foreign contaminants or ester decomposition to the carboxylic acid. These checks confirmed the initial purity of all three methyl-anthroates.

In later work, unexpected fine structure did appear in the fluorescence spectrum of methyl-9-anthroate. Dilution of the sample increased the fine structure thereby signaling that decomposition of the ester to the acid, which would dissociate in dilute ethanol to give the observed fine structure, had occurred. To get rid of the anthroic acid anion, 9-COOME was purified by the following steps:

1) Suspension in a 10% NaOH solution with stirring
2) Washing with large amounts of water
3) Washing with a small amount of cold ethanol
4) Drying in a hot air oven

This procedure was repeated until the fine structure due to the presence of the acid decomposition product in ethanol was not observed at the highest sample sensitivity setting of the fluorometer.

Solvents: Cyclohexane and absolute ethanol were supplied by Fisher Scientific and U.S. Industrial Chemicals respectively. Spectral grade acetonitrile was either Eastman or Matheson, Coleman, and Bell. Hexane, N,N-dimethyl formamide, dimethyl sulfoxide, ethyl acetate, butyl acetate, and isopropanol were all Matheson, Coleman, and Bell Spectroquality or Omnisolv grade. Tetrahydrofuran was Mallinckrodt analytical grade. Purification was required for hexane, Eastman acetonitrile, tetrahydrofuran, and ethanol.

Hexane was distilled from Matheson, Coleman, and Bell Molecular Sieve type 4A to remove contaminants.

Eastman acetonitrile was treated to remove water that had been picked up on standing by running the solvent through a buret containing type 4A molecular sieve. However, an absorbance spectrum of this dry acetonitrile still showed the presence of impurities. Therefore, distillation from approximately one gram of Fisher Scientific calcium hydride was undertaken. Significant improvement was observed in the absorbance spectrum following distillation. A second distillation further increased purity. Fresh MCB acetonitrile was found suitable for spectral work without the above purification steps.

Tetrahydrofuran was treated to remove both peroxides and water. To remove trace peroxides, a .5% suspension of cuprous chloride in THF was refluxed for thirty minutes and

then distilled. Water was removed by a second distillation from calcium hydride.

Before use in quantum yield determinations, absolute ethanol was distilled from calcium hydride to assure dryness.

Finally, for each solvent, a fluorescence scan from 380 to 600 nm was run to guarantee the absence of fluorescent contaminants under the conditions to be used for the solvents.

Instrumentation: Sample absorbances and absorption spectra were obtained either on the Beckman DU or the Cary 118C Spectrophotometer. From a table of representative compounds supplied with the Cary 118C, anthracene was found to have an approximate natural bandwidth of 3 nm and an optimal spectral bandwidth of .3 nm. For our study using substituted esters of anthracene, a comparable spectral bandwidth was used to calculate a slit setting of .02 mm. The Cary was operated in the auto gain mode at all times.

The thermostatted sample cell of the Cary 118C was used for all of the absorbance versus temperature work. Figure 2 shows a diagram of the controlled temperature cell setup used for the absorbance versus temperature work. A P.M. Tamson Company Type T.Z. 9/100 thermostatted water bath controlled the Cary cell block temperature. Measurement of the exact temperature in the sample cell was achieved by suspending a copper-constantan thermocouple attached to

Figure 2

Thermostatted Cell Compartment of the Cary 118C

A quartz cell was placed in the thermostatted cell block of the Cary 118C which had water from the constant temperature bath circulating through it. A copper-constantan thermocouple attached to an Omega 2160A digital thermometer was suspended directly in the sample cell.

THERMOCOUPLE

RUBBER STOPPER

TO BATH
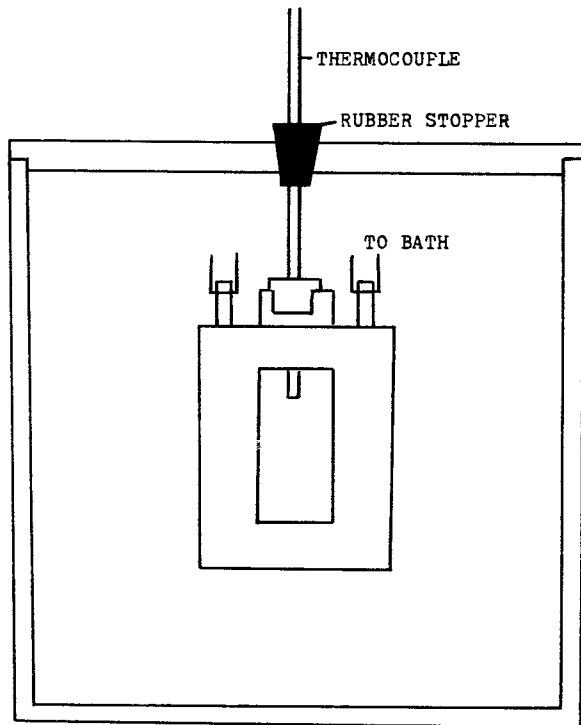
an Omega 2160A digital thermometer directly in the sample
cell. To allow this, it was necessary to drill a hole in
the cell compartment cover of the Cary 118C. The thermo-
couple was inserted through a rubber stopper which in turn
was inserted securely in the hole in the cell compartment
cover. The tapered rubber stopper did not allow any light
leaks into the cell compartment. The teflon cap of the
sample cell was also drilled to allow passage of the thermo-
couple into the sample solution.

Uncorrected fluorescence spectra were recorded on the
Hitachi Perkin-Elmer MPF-2A Spectrofluorometer. Wavelength
calibration and light source alignment adjustments were made
to ensure optimal data. When necessary, corrections for
photomultiplier and emission monochromator response were
applied as described by Werner and Hoffman.[10] Corrections
for the xenon arc lamp intensity and excitation monochromator
response were obtained using a rhodamine B quantum counter.[11]

To study the temperature dependence of the fluorescence
quantum yield, the thermostatted cell block supplied by
Perkin-Elmer was used. A 95% ethanol bath regulated by an
FTS Systems Flexicool unit as diagrammed by Hawkins was used
for temperature control.[6] Actual temperature measurements
were made in the cell block of the fluorometer using the
copper-constantan thermocouple inserted in a cell containing
n-butanol. This cell was placed in the cell compartment

directly adjacent to the sample cell compartment being irradiated. Hawkins has reported no detectable difference in temperature between various positions in the cell holders of the thermostatted cell block.[6] The thermocouple was attached to the Omega 2160A digital thermometer for easy temperature reading.

Procedure: Quantum yield determinations followed the revised procedure by Werner.[12] At room temperature, the quantum yield of an unknown compound can be related to that of a reference compound by equation 4.

$$\phi_{f,u} = \phi_{f,r} * \frac{A_r * F_u * AF_u * DF_u * I_r * n_u^2}{A_u * F_r * AF_r * DF_r * I_u * n_r^2} \tag{4}$$

where:

r= reference compound
u= unknown compound
A= absorbance at exciting wavelength
F= area under uncorrected fluorescence spectrum
AF= area correction factor
DF= degassing factor for oxygen quenching
I= xenon source intensity at exciting wavelength
n= refractive index of the solvent

The reference used was methyl-9-anthroate in ethanol ($\phi_{f,r}$= .173). A Keuffel and Esser Model 60 0002 Compensating Polar Planimeter was used in determining the area under the fluorescence curves. Area correction factors were calculated as the ratio of the area of the corrected fluorescence spectrum to the area of the uncorrected fluorescence spectrum. The degassing factor is the ratio of the uncorrected fluorescence intensity at the wavelength maxima of a deoxygen-

ated sample to that for an oxygen equilibrated solution. Relative lamp intensities at the wavelength of excitation were read from the xenon lamp profile obtained from a rhodamine B quantum counter.

For determining the quantum yield of a given compound as a function of temperature, equation 4 simplifies to equation 5 using the room temperature quantum yield as a reference.

$$\phi_f(T) = \phi_f(RT) * \frac{A_{RT} * F_T * n_T^2}{A_T * F_{RT} * n_{RT}^2} \tag{5}$$

where:

RT= room temperature
T= temperature of interest

The absorbance at the exciting wavelength has a temperature dependence that lends appreciable error to the quantum yield determination if unaccounted for. The absorbance decreases almost linearly as temperature is increased due to solvent expansion. However, absorbance corrections for temperature were required only for those sample solutions whose fluorescence versus temperature work was recorded while exciting at a wavelength corresponding to a peak, either the 0-1 or 0-2 vibronic band, in the absorption spectrum. If the fluorescence versus temperature work was recorded whi   xciting at a wavelength corresponding to a valley between vibronic bands in the absorption spectrum, the absorbance temperature correction was unnecessary.

Facci has shown the valley absorbance to be relatively in-
sensitive to temperature with a change of only 1% over the
range of temperatures used.[7]

Unlike the room temperature quantum yield determination
procedure, the area under the uncorrected fluorescence
curve was not used as a measure of F in equation 5. A di-
rect correlation between the uncorrected maximun intensity
of fluorescence and the uncorrected area was found when the
two were compared. This allowed the use of the maximum in-
tensity measured from the spectral baseline to be used as
a measure of F.

To obtain the fluorescence intensities as a function
of temperature, deoxygenated samples were used because in-
creases in temperature increase the rate of oxygen diffusion
and facilitate quenching of fluorescence. The freeze-thaw
degassing procedure has been described by Hawkins with
modifications by Facci.[6,7] The pressure was reduced to
less than $5*10^{-4}$ Torr during each pump cycle as read from
a Varion ion gauge. For each ester/solvent pair, at least
two samples with an absorbance of less than .05 at the
exciting wavelength were degassed in pyrex cells, and from
two to four temperature runs were recorded on each. At
least 8-10 fluorescence intensities over a 40-50°C temper-
ature range constituted a run, with one intensity always
being at room temperature (23°C). The ratio mode of the
fluorometer was used to collect data for these runs. When

the digital thermometer signaled a temperature at which a
fluorescence intensity was to be recorded, the fluorometer
was scanned over the peak of maximum emission. If fluores-
cence intensities were record 1 at temperatures below $15^{\circ}C$,
cold nitrogen was blown through the cell compartment to
prevent frosting of the sample pyrex cell.

The final factor in equation 5 that requires attention
in determining the quantum yield as a function of tempera-
ture is the refractive index change. The change in refrac-
tive index with temperature is calculated using equation 6.

$$n_T = n_{RT} + dn/dt * \Delta t \qquad (6)$$

Values for dn/dt for some solvents were available in the
literature, while those for other solvents were calculated
from literature refractive index measurements listed at two
different temperatures.[13]

As previously mentioned, absorbance versus temperature
work was necessary for samples excited at an absorption
peak during the fluorescence versus temperature experimental
work. For this procedure, samples were made with an absorb-
ance of approximately 1.0 at the excitation wavelength. This
absorbance range was picked merely for convenience. All
samples used in the fluorescence versus temperature work
had absorbances of less than .05 at the excitation wave-
length. It has been reported, however, that the absorbance
correction does not change appreciably with the absolute

value of the room temperature absorbance.[6] Using the
apparatus described earlier, absorbance readings were taken
at the same temperatures used in the fluorescence versus
temperature work after zeroing the Cary 118C at 450 nm,
where the samples do not absorb. This allowed calculation
of Abs(23)/Abs(T) values to be included in equation 5.

There was some concern that the Abs(23)/Abs(T) values
calculated using absorbances read from the Cary could not
be used to correct relative fluorescence intensities due to
the vast difference in spectral bandwidths between the Cary
(.3 nm) and the fluorometer (7 nm). Therefore, an addition-
al procedure was undertaken to find the dependence of absorb-
ance versus temperature correction on spectral bandwidth.
Absorbance versus temperature data were recorded for a sam-
ple of methyl-1-anthroate in acetonitrile using slit settings
of both .02 mm and .2 mm. Table 1 gives the results for this
work. At alltemperatures, agreement in the absorbance read-
ings to three significant figures shows that increasing the
slit width by a factor of ten has very little effect on the
absorbance. From this finding, it was concluded that the
disparity between the spectral bandwidths of the Cary 118C
and the fluorometer should create no serious problems.

With the guidance of Dr. Gregory D. Gillespie, SUNY at
Albany, and the use of his laboratory, some additional
procedures were undertaken in attempts to find the position

Table 1

Absorbance Versus Temperature Data for Methyl-1-Anthroate

in Acetonitrile as a function of Slit Width

Temperature ($^\circ$C)	Absorbance[a] Slit=.02mm	Absorbance[a] Slit=.2mm
18	1.1071	1.1087
23	1.0981	1.0998
28	1.0895	1.0914
33	1.0818	1.0827
38	1.0932	1.0915
43	1.0803	1.0850
48	1.0767	1.0792
53	1.0670	1.0640
58	1.0538	1.0506
63	1.0388	1.0363

(a) excitation wavelength= 372 nm

of the triplet energy levels in the three methyl-anthroates.
Total and delayed emission spectra were recorded on a few
samples in an attempt to detect the presence of triplet-
triplet fluorescence and phosphorescence respectively. The
samples had been carried through six freeze-thaw degassing
cycles to thoroughly eliminate oxygen. The spectra were
measured with a photon counting spectrofluorometer equipped
with a photomultiplier sensitive to approximately 860 nm.
All total and delayed emission spectra were run at room
temperature. Delayed emission was also recorded at liquid
nitrogen temperature ($77^{\circ}K$) for a couple of samples.

RESULTS

RESULTS

Room temperature quantum yields (ϕ_f@ 22 or 23°C) were calculated as discussed previously. Table 2 lists the degassing factors (DF), area correction factors (AF), and solvent refractive index values (n_D) used in the quantum yield determinations. The results of the room temperature quantum yield calculations are summarized in Table 3.

Activation energies (E_a) were obtained from the fluorescence versus temperature data by a least squares computer program which fit the data to an Arrhenius expression (log ($\phi_f^{-1}-1$)=log A-E_a/2.303RT). The suitability of this expression will be discussed later. The program is explained in detail in Appendix I. The refractive index change with temperature values (dn/dt) used to calculate quantum yields as a function of temperature are given in Table 2. Overall, the Arrhenius plots show good linearity with correlation coefficients usually greater than .9900. Activation energies were not determined when the room temperature quantum yield for a given ester in a given solvent exceeded approximately .85. For these high quantum yield values, the error introduced in the activation energy determination is very large and negates the use of the values obtained.

Mean wavenumbers of fluorescence ($\overline{\nu}_f$) were determined by a second computer program outlined in Appendix II, and the results are included in Table 3. For each ester in

Table 2

Degassing Factors, Area Correction Factors, Solvent Refractive Index, and Refractive Index Change with Temperature Values for the Ester/Solvent Pairs

Compound/ Solvent	DF	AF	$n_D(^{\circ}C)$	dn/dt
Methyl-1-anthroate				
cyclohexane	1.06	.87	1.424616(23)	-.000538
butyl acetate	1.24	.911	1.39261(23)	-.00047
tetrahydrofuran	1.22	.927	1.40628(22)	-.00044
dimethyl formamide	1.31	1.00	1.42938(22)	-.00046
acetonitrile	1.69	.99	1.34321(22)	-.00045
Methyl-2-anthroate				
hexane(a)	1.70	.79	1.372692(22)	-.000542
cyclohexane(a)	1.41	.84	1.42623(22)	-.000538
butyl acetate	1.78	.823	1.38850(23)	-.00047
tetrahydrofuran	1.62	.821	1.40628(22)	-.00044
dimethyl formamide	1.36	.87	1.42938(22)	-.00046
Methyl-9-anthroate				
cyclohexane	1.31	.92	1.42623(22)	-.000538
butyl acetate	1.42	.970	1.39261(23)	-.00047
tetrahydrofuran	1.46	.990	1.40628(22)	-.00044
dimethyl formamide	1.21	1.05	1.42938(22)	-.00046
dimethyl sulfoxide	1.04	1.09	1.4760(22)	-.0002
acetonitrile(a)	1.26	1.03	1.34321(22)	-.00045
ethanol	1.16	1.13	1.360218(23)	-.000404
ethyl acetate	1.49	.990	1.37141(22)	-.00049
isopropanol	--	--	1.3760(23)	-.0004

(a) See Reference 9

Table 3

Room Temperature Quantum Yields, Activation Energies, Mean Wavenumbers of Fluorescence and Log(A/k_f) Values for the Ester/Solvent Pairs

Compound/ Solvent	$\bar{\nu}_f*10^4$ (cm^{-1})	ϕ_f (22 or 23°C)	E_A (kcal/mole)	Log(A/k_f)
Methyl-1-anthroate[a]				
cyclohexane(33)	2.31	.12±.003	2.20±.04	2.482
butyl acetate	2.24	.41±.02	3.47±.06	2.717
tetrahydrofuran(37.4)	2.22	.46±.01	3.77±.10	2.849
acetonitrile(46)	2.17	.81±.01	5.17±.12	3.180
dimethyl formamide(43.8)	2.16	.95±.01	-	-
Methyl-2-anthroate				
hexane(30)	2.39	.33±.01[b]	2.74±.08	2.326
cyclohexane(33)	2.38	.47±.02[b]	3.53±.17	2.633
butyl acetate	2.35	.92±.02	-	-
tetrahydrofuran(37.4)	2.33	.96±.03	-	-
dimethyl formamide(43.8)	2.29	.84±.01	-	-
Methyl-9-anthroate				
cyclohexane(33)	2.23	.76±.01	2.67±.06	1.467
butyl acetate	2.19	.72±.01	3.03±.10	1.814
ethyl acetate	2.18	.66±.01	3.85±.34	2.542
tetrahydrofuran(37.4)	2.18	.82±.02	-	-
acetonitrile(46)	2.15	.39±.03[b]	4.11±.06	3.231
dimethyl formamide(43.8)	2.14	.70±.01	4.53±.12	2.972
dimethyl sulfoxide	2.12	.56±.01[b]	3.98±.04	2.827
isopropanol(48.6)	2.11	.24±.02[b]	3.78±.21	3.292
ethanol(52)	2.10	.173±.008	4.27±.13	3.826

(a) E_T(30) values- empirical solvent polarity scale[14]
(b) ϕ_f determinations by Matthews[9]

Table 3, the solvents used are listed in order of decreasing mean wavenumbers of fluorescence. This red shift in fluorescence, as measured by the mean wavenumber, shows the solvent dependence of the first excited singlet state (S_1), from which fluorescence originates. $E_T(30)$ values, an empirical solvent polarity scale, are listed after each solvent for which a value is available. A comparison of mean wavenumber with the empirical solvent polarity scale $(E_T(30))$ in Figure 3 reveals a general decrease in $\bar{\nu}_f$ with increasing polarity for all three methyl-anthroates, although exceptions can be noted.

Using the data in Table 3, plots of the room temperature quantum yield versus mean wavenumber of fluorescence (Figures 4,5), activation energy versus mean wavenumber of fluorescence (Figures 6,7), and room temperature quantum yield versus activation energy (Figure 8) were constructed.

Note in Figures 4 and 6, the quantum yield and activation energy both increase as S_1 energy decreases for methyl-1-anthroate. In Figure 8, 1-COOME shows a highly linear relation between the room temperature quantum yield and activation energy. A correlation coefficient of .999 was calculated for a line joining the four points for 1-COOME in Figure 8.

Similar to the methyl-1-anthroate data, methyl-2-anthroate shows an increase in quantum yield with decreasing S_1

Figure 3

$E_T(30)$ versus $\overline{\nu}_f$ for 1-COOME, 2-COOME, and 9-COOME

Comparing the mean wavenumber of fluorescence ($\overline{\nu}_f$) with the empirical solvent polarity scale ($E_T(30)$) , we see a general decrease in $\overline{\nu}_f$ with increasing polarity for all three methyl-anthroates.

Solvent Key

A - acetonitrile
DMF - dimethyl formamide
THF - tetrahydrofuran
C - cyclohexane
H - hexane
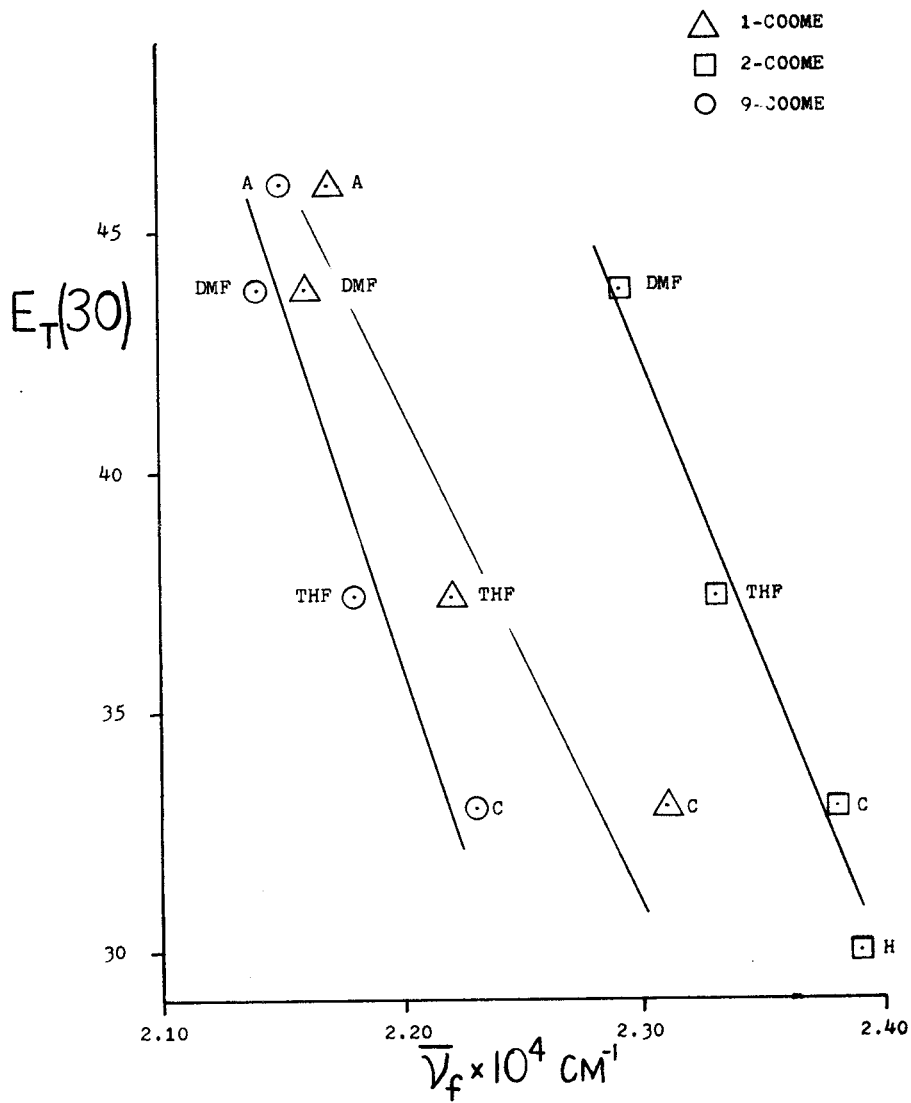
Figure 4

ϕ_f versus $\overline{v}_f$ for 1-COOME and 2-COOME

For 1-COOME, ϕ_f increases linearly as S_1 energy de-creases. For 2-COOME, ϕ_f increases as S_1 energy decreases up to tetrahydrofuran. Then, in going to dimethyl formamide, the ϕ_f for 2-COOME decreases.

Solvent Key

A - acetonitrile
DMF - dimethyl formamide
THF - tetrahydrofuran
BA - butyl acetate
C - cyclohexane
H - hexane
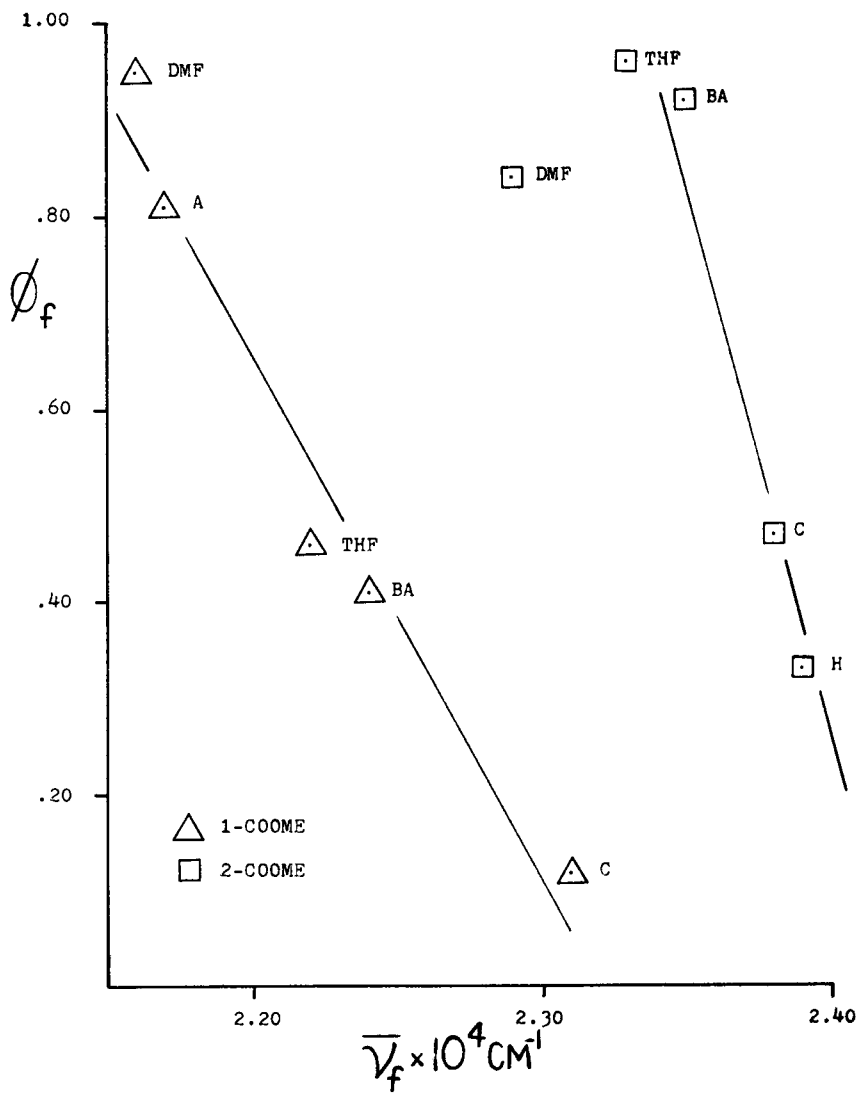
Figure 5

$$\emptyset_f \text{ versus } \overline{\nu}_f \text{ for 9-COOME}$$

Although scatter exists, 9-COOME shows a general decrease in $\emptyset_f$ as S_1 energy decreases.

Solvent Key

A - acetonitrile
DMSO - dimethyl sulfoxide
EA - ethyl acetate
DMF - dimethyl formamide
BA - butyl acetate
THF - tetrahydrofuran
C - cyclohexane
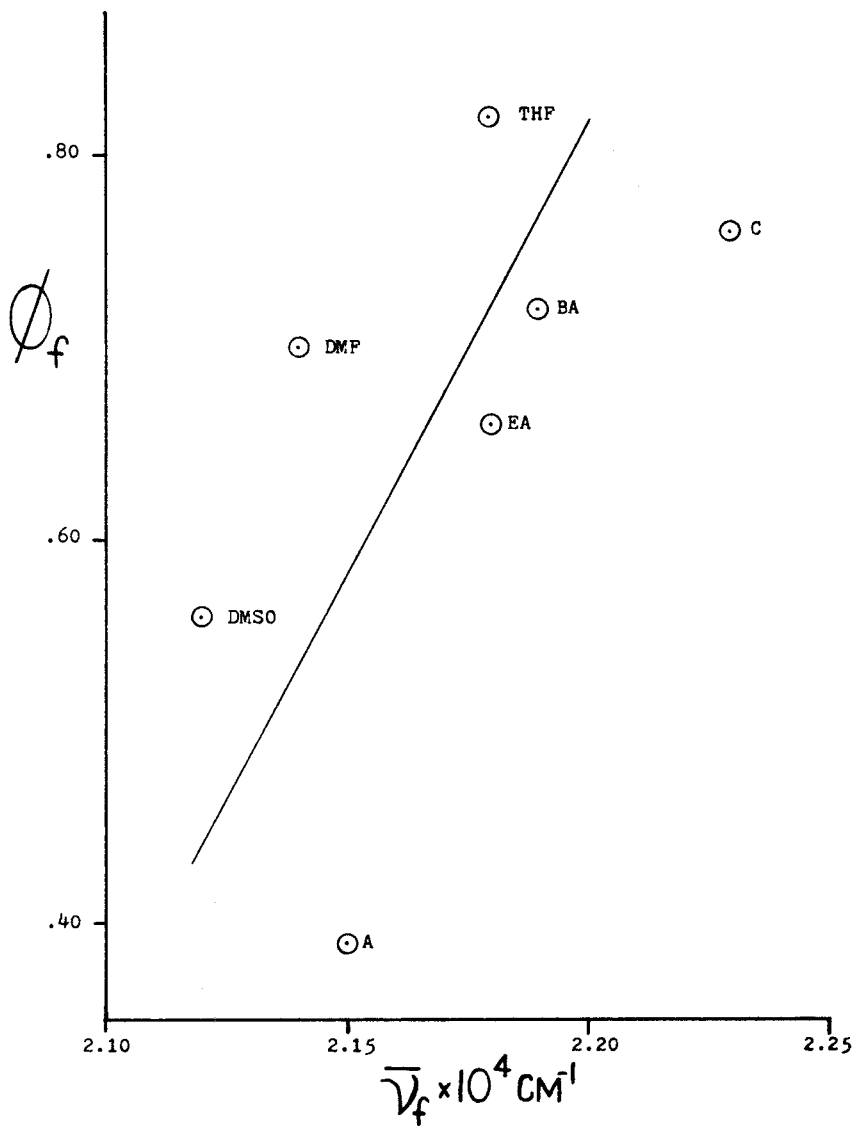
Figure 6

E_a versus $\overline{\nu}_f$ for 1-COOME and 2-COOME

For 1-COOME, E_a increases linearly as S_1 energy decreases. For 2-COOME, only two activation energies are available, but the two show an increase as S_1 energy decreases.

Solvent Key

A - acetonitrile
THF - tetrahydrofuran
BA - butyl acetate
C - cyclohexane
H - hexane
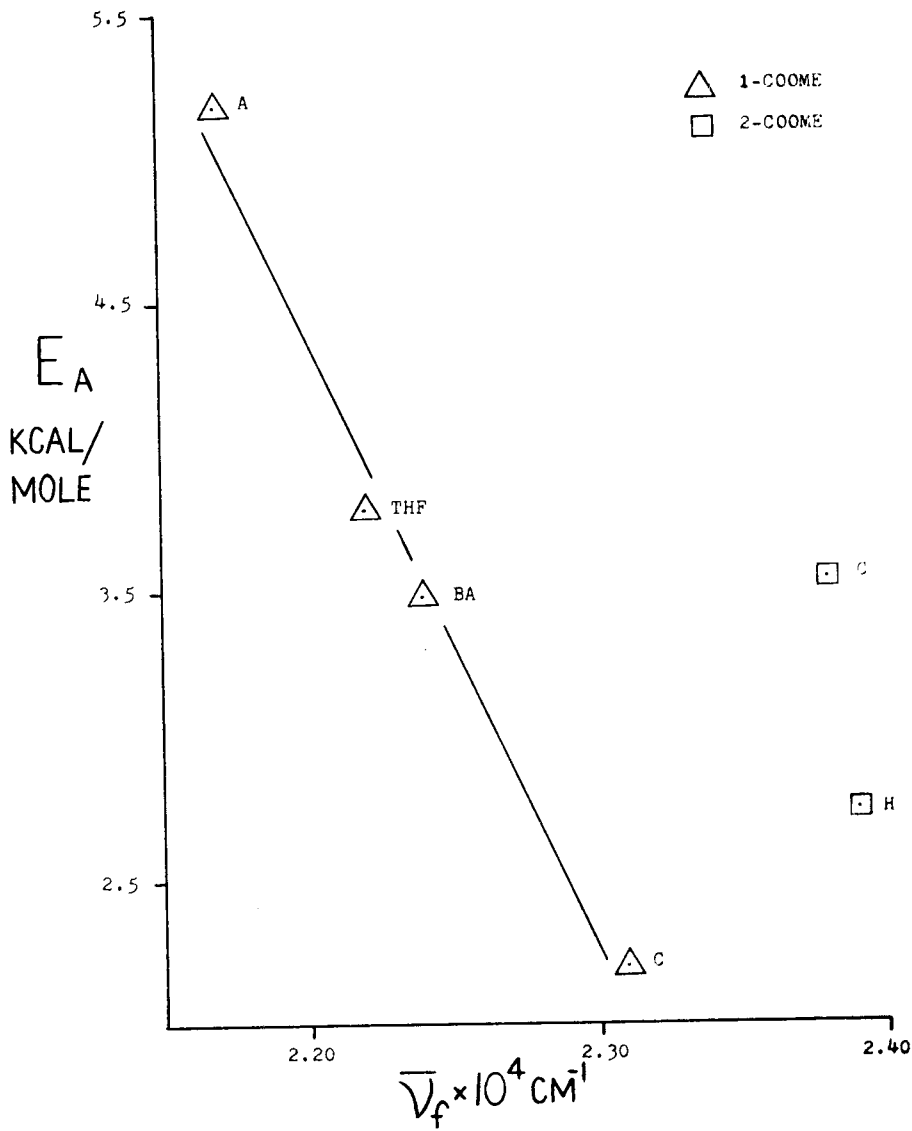
Figure 7

E_a versus $\overline{\nu}_f$ for 9-COOME

9-COOME shows the same general trend of increasing E_a with decreasing S_1 energy as is exhibited by both 1 and 2-COOME.

Solvent Key

DMF - dimethyl formamide
A - acetonitrile
DMSO - dimethyl sulfoxide
EA - ethyl acetate
BA - butyl acetate
C - cyclohexane
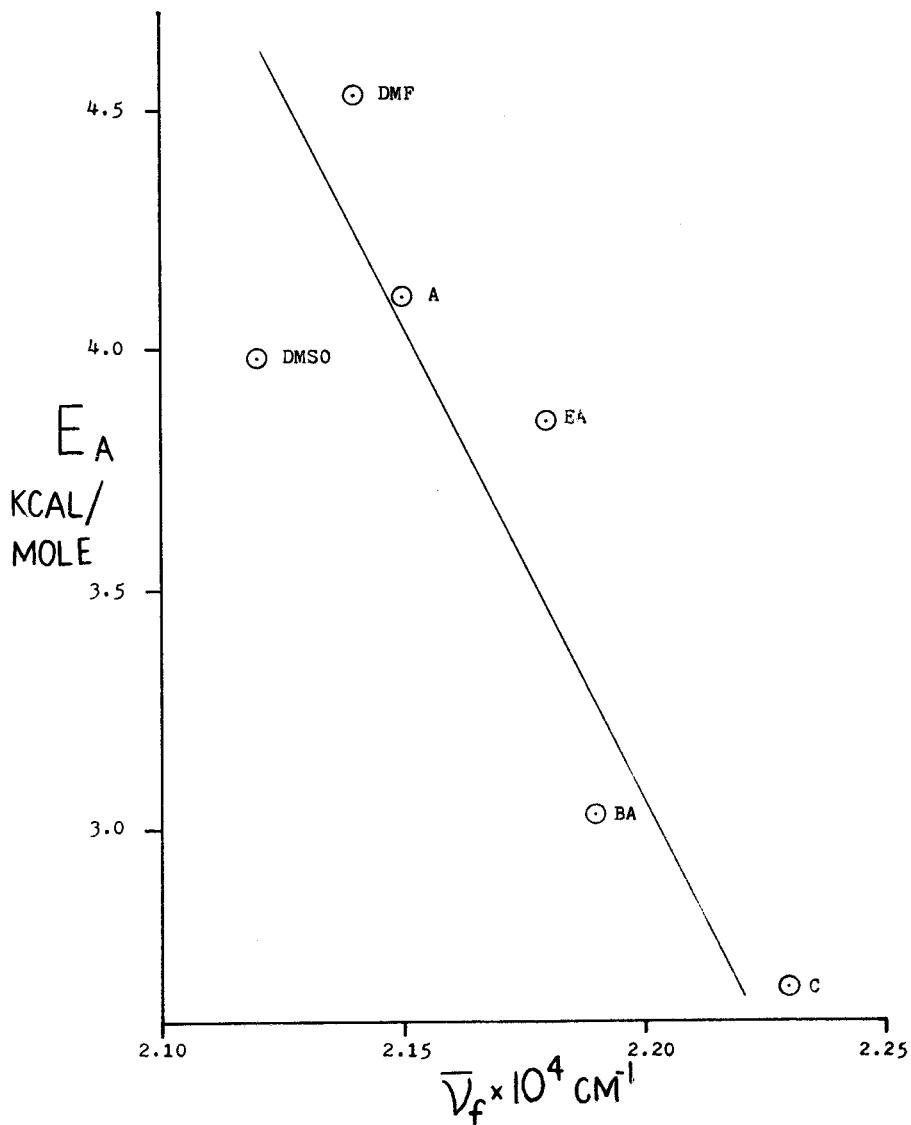
Figure 8

ϕ_f versus E_a for 1-COOME, 2-COOME, and 9-COOME

1-COOME and 2-COOME show a highly linear relation of increasing ϕ_f with increasing E_a. In contrast, although no highly linear correlation between ϕ_f and E_a exists for 9-COOME, a general decrease in ϕ_f with increasing E_a can be seen.

Solvent Key

C - cyclohexane
A - acetonitrile
BA - butyl acetate
EA - ethyl acetate
DMF - dimethyl formamide
DMSO - dimethyl sulfoxide
THF - tetrahydrofuran
H - hexane
I - isopropanol
E - ethanol
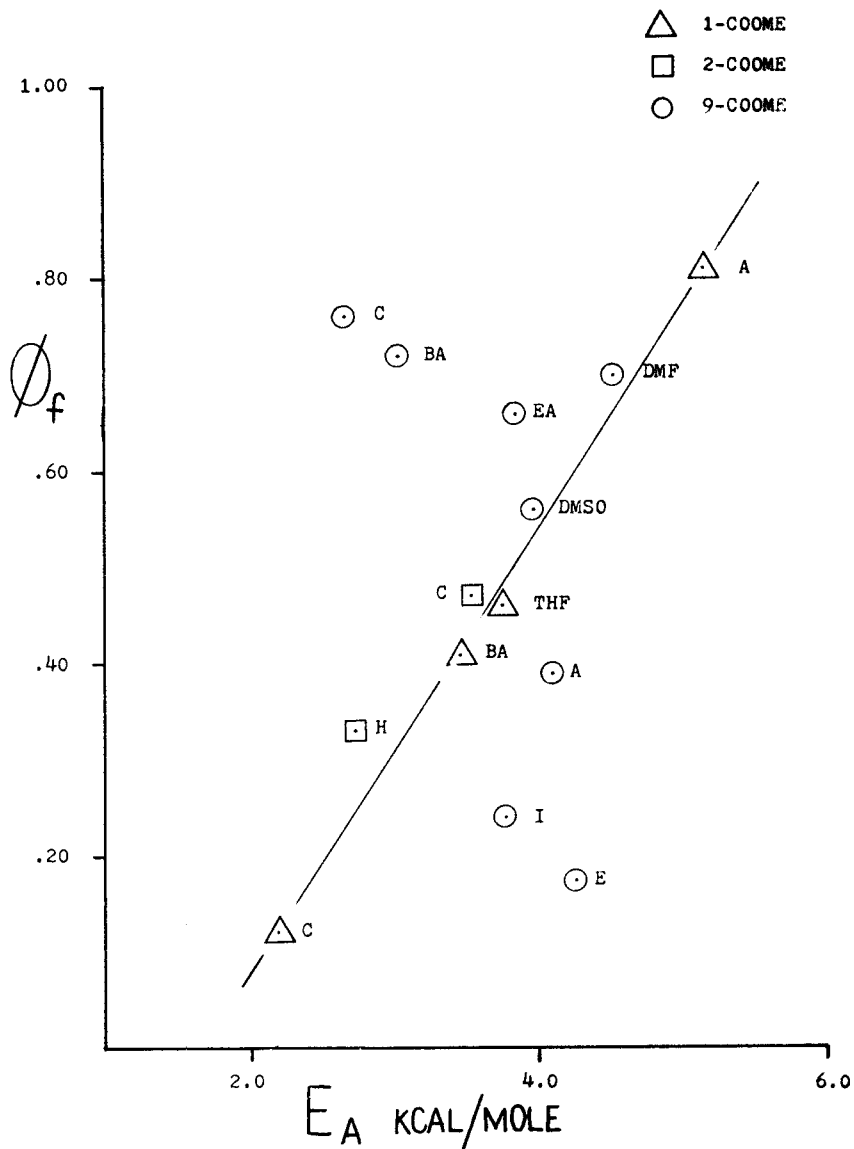
energy in quite nonpolar solvents (Figure 4). However, unlike 1-COOME, the quantum yield for 2-COOME reaches a maximum in tetrahydrofuran and then drops in going to dimethyl formamide. Although activation energies are available only for the very nonpolar solvents hexane and cyclohexane, an increase in E_a is noted as S_1 energy decreases, just as for 1-COOME (Figure 6). In Figure 8, if the two points for 2-COOME are included with those for 1-COOME, a correlation coefficient of .986 is obtained for the linear relation between quantum yield and activation energy for both of these esters.

In contrast to the previous esters, methyl-9-anthroate shows a general decrease in quantum yield with decreasing mean wavenumber of fluorescence, although considerable scatter exists (Figure 5). From Figure 7, we can see the same general trend of increasing activation energy with decreasing S_1 energy for 9-COOME as is exhibited by both the 1 and 2 substituted esters. In the plot of quantum yield versus activation energy (Figure 8), 9-COOME shows a rather diffuse collection of points. Unlike the data for 1 and 2-COOME, the plot of $\emptyset_f$ versus E_a for 9-COOME shows no highly linear relation.

As previously mentioned, absorbance versus temperature correction values had to be determined for samples excited at an absorption peak during the fluorescence versus tem-

perature experimental work. Table 4 lists the absorbance
correction factor values for the five ester/solvent pairs
requiring this correction. Note the general trend of in-
creasing Abs(23)/Abs(T) values due to decreasing absorbances
when the temperature is increased for all five combinations.

As mentioned previously, emission spectra for several
ester/solvent pairs were recorded on a photon counting flu-
orometer at SUNY at Albany. For all of the samples examined,
no triplet-triplet fluorescence or phosphorescence were iden-
tifiable in the total or delayed emission spectra respectively.
Methyl-1-anthroate in cyclohexane showed the possibility
of a phosphorescence peak at approximately 660 nm for the
degassed sample. However, after breaking the sample open
to allow oxygen equilibration, the same peak appeared in the
delayed emission spectrum ruling out phosphorescence. Oxygen
quenching would have eliminated phosphorescence if it were
truly present. Delayed emission spectra of methyl-1-anthroate
at $77^{\circ}K$ in both cyclohexane and methylcyclohexane, a glass
forming solvent, contained the 660 nm peak which was iden-
tified to be a pyrex emission from the sample cell.

Since no triplet-triplet fluorescence or phosphorescence
could be found for any of the three esters used in this
study, no information on the location of the energy levels
in the triplet manifold was gained. It was hoped this in-
formation would elucidate whether our activation energy

Table 4

Absorbance versus Temperature Correction Values

Temperature (°C)	Abs(23)/Abs(T)				
	9-COOME/ butyl acetate	9-COOME/ dimethyl formamide	9-COOME/ dimethyl sulfoxide	1-COOME/ aceto- nitrile	1-COOME/ butyl acetate
13	-	.976	-	-	-
18	-	.986	.998	.992	.995
23	1.	1.	1.	1.	1.
28	1.014	1.014	1.009	1.011	1.006
33	1.027	1.024	1.015	1.022	1.017
38	1.039	1.033	1.020	1.038	1.026
43	1.050	1.051	1.024	1.049	1.030
48	1.061	1.062	1.037	1.057	1.035
53	1.070	1.080	1.049	1.069	1.041
58	1.078	1.096	1.062	1.077	1.046
63	1.097	1.117	1.075	1.085	1.052
68	1.101	-	1.088	-	-

calculations were truly a measure of the S_1-T_x energy gap which must be overcome for intersystem crossing to occur.

DISCUSSION

DISCUSSION

As introduced previously, this study was undertaken
to investigate the observed solvent dependence of the fluo-
rescence quantum yield for the three monosubstituted methyl
esters of anthroic acia. Earlier work by Hawkins and Facci
has suggested that thermally assisted intersystem crossing
to a triplet level near S_1 may become efficient in certain
solvents and compete with fluorescence in deactivating S_1.[6,7]
This pathway would result in a variation in quantum yield
as a function of solvent.

Information on the positioning of such a triplet energy
level would be invaluable in assessing the probability of
the proposed solvent sensitive intersystem crossing process.
As previously described, attempts were made to locate the
triplet energy levels in the methyl-anthroates. Our failure
to gain any insight on the triplet manifold is not surpris-
ing when one considers the odds we were working against.
At room temperature, oxygen quenching may still effect phos-
phorescence despite thorough degassing involving six freeze-
thaw degassing cycles. At low temperatures, the quantum
yields of the esters approach unity so that the number of
molecules that may intersystem cross may be negligible.
Furthermore, triplet-triplet fluorescence and phosphorescence,
if they do occur, have very low yields and occur at wave-
lengths for which even the most sensitive photomultiplier

would have difficulty detecting them on the tailing edge
of the normal fluorescence spectrum. Therefore, we are
resigned to making assumptions about the triplet manifold
for our model of the radiative and nonradiative processes
of methyl-anthroates.

Since efforts to assign the position of the triplet
levels failed for the three methyl esters, information on
the triplet levels of the parent compound, anthracene, and
its derivatives will be used as a starting point to help
rationalize the trend of quantum yield with solvent. In
anthracene, the S_1 energy level lies close to and slightly
higher in energy than a nearby triplet level, probably T_2.
The fluorescence spectrum of anthracene gives an S_1 energy
of $26,700$ cm^{-1}, [6,15] and triplet-triplet absorption places
T_2 at $26,050$ cm^{-1}. [15] The lowest triplet, T_1, has been
located in anthracene via phosphorescence and lies much
lower in energy ($14,700$ cm^{-1}). [15] Substitution on anthra-
cene increases the area over which electrons are delocalized
and also destroys some of its symmetry. Therefore, substi-
tution increases the polarity of S_1 by charge-transfer
effects and lowers the S_1 energy relative to the ground
state, S_0. In contrast, Becker has found the triplet mani-
fold in anthracene to be less sensitive to substitution for
methyl and dichloro derivatives. [15] Donckt has reported
triplet states are generally less affected by charge-transfer

effects than excited singlet states.[16] Also, anthracene's triplet manifold is less sensitive to changes in solvent. Wu and Ware have found S_1 to be considerably stabilized by solvent while T_2 is stabilized to a lesser extent (30% of that on S_1) for 9,10-dibromoanthracene.[17] Therefore, using anthracene and its derivatives as points of reference, the assumptions that the energies of the triplet manifold do not vary significantly with substituent or with solvent will be adopted for the carboxyl substituted anthracenes used in this study.

Many studies have been undertaken on the photophysical processes that occur in anthracene and its derivatives. Others have found the fluorescence rate constant, k_f, to be temperature independent for anthracene and several of its derivatives over a wide temperature range.[18,19] Additionally, the fluorescence rate constant has been found to be relatively independent of solvent except for a slight refractive index dependence.[6,7,9] Hence, k_f is a molecular property relatively independent of temperature and solvent.

Generally, two nonradiative processes, internal conversion and intersystem crossing, compete with fluorescence in deactivating S_1. For anthracene and its derivatives, however, quenching experiments by Medinger and Wilkinson,[20] deuteration experiments by Laposa,[21] and triplet occupation quantum yields by Bennett and McCartin[19] have all shown

internal conversion to be negligible. We therefore assume
that only fluorescence and intersystem crossing affect S_1
in methyl-anthroates. The quantum yield of anthracene has
been found to be relatively independent of solvent. In
contrast, our data show that the quantum yield of the methyl
esters are very dependent on solvent. Recall, S_1 is quite
solvent sensitive while the triplet manifold is expected to
show a lesser solvent dependence. Unlike anthracene, in
which S_1 lies slightly above T_2, S_1 may lie below a nearby
triplet, call it T_x, for methyl-anthroates. If this is the
case, the quantum yield will be dependent on temperature
since intersystem crossing will require thermal activation.
Our data show a decrease in quantum yield with increasing
temperature for all three methyl-anthroates in a variety of
solvents. Thus, we expect S_1 is below T_x and postulate that
the S_1-T_x energy gap may explain the observed solvent de-
pendence of the quantum yield for methyl-anthroates.

Drawing together our assumptions and findings thus far,
a simple model can be constructed on three major premises
to predict the fluorescence behavior of the three methyl
esters of anthroic acid.

1) Since the position of S_1 is dependent on solvent
while the triplet levels should be relatively un-
effected, we expect the quantum yield for a given
ester to increase due to a solvent induced lowering
of S_1 and consequent increase in the S_1-T_x energy
gap for intersystem crossing.

2) Using the activation energy (to be discussed more

fully later) as a measure of the S_1-T_x energy gap, we expect an increasing activation energy with decreasing S_1 energy due to the increased S_1-T_x gap.

3) Since we expect both $\emptyset_f$ and E_a to increase with decreasing S_1 energy, the two quantities should be correlated: That is, as E_a increases, so should $\emptyset_f$.

Recall, all three methyl-anthroates show a decrease in quantum yield with increasing temperature. Since, for anthracene derivatives, k_{ic} is negligible and k_f is temperature independent, the temperature dependence of $\emptyset_f$ must reside in k_{isc}. Therefore, it seems reasonable that if k_{isc} can be fit by the Arrhenius relation, the resulting activation energy for intersystem crossing (E_a) may be a rough measure of the gap between S_1 and the nearby triplet to which crossing occurs ($E_{S_1-T_x}$).

Generally, the relationship between k_{isc} and temperature is given by equation 7, where k^o_{isc} is the temperature in-

$$k_{isc} = k^o_{isc} + Ae^{-E_a/RT} \qquad (7)$$

dependent intersystem crossing rate constant. The value of $\emptyset_f$ as a function of temperature is given by equation 1. Insertion of equation 7 into equation 1 with the elimination of k_{ic} from the denominator ($k_{ic} \ll k_f, k_{isc}$) leads, upon rearrangement, to equation 8, where $\emptyset^o_f$ is the low temperature

$$\log(1/\emptyset_f - 1/\emptyset^o_f) = \log(A/k_f) - E_a/2.303RT \qquad (8)$$

limit for the quantum yield as given by equation 9. If we

$$\emptyset^o_f = k_f/(k_f + k^o_{isc}) \qquad (9)$$

assume $\emptyset^o_f$ to be unity, equation 8 simplifies to equation 10

$$\log(1/\emptyset_f(T) - 1) = \log(A/k_f) - E_a/2.303RT \qquad (10)$$

and a plot of $\log(1/\emptyset_f - 1)$ versus $1/T$ will be linear yielding E_a from the slope and $\log(A/k_f)$ from the intercept.

Nevertheless, the validity of fitting the $\emptyset_f$ versus temperature data to equation 10 relies on several assumptions. If a plot of $\log(1/\emptyset_f - 1)$ versus $1/T$ yields a straight line, the assumption that just one temperature dependent process (ISC) competes with fluorescence is supported. However, a straight line could also result from the unlikely case that two processes with the same activation energy compete with fluorescence in deactivating S_1. The assumption that $\emptyset_f$ goes to unity at low temperatures (IC negligible) seems reasonable from our findings that for several ester/solvent pairs, $\emptyset_f$ is within experimental error of unity around 0^oC. Correlation coefficients near unity ($>.9900$) for the aforementioned Arrhenius plots lead us to believe, for our anthroate esters, that Arrhenius behavior of k_{isc} is a realistic expectation.

The measurement of an activation energy implies that there is a minimum threshold energy below which intersystem crossing vanishes.[22] Below this energy the probability of crossing to T_x is zero, and above it the transition probability is some finite value. In our model for the fluorescence behavior of the three methyl-anthroates, we assume that E_a is a measure of the $S_1 - T_x$ energy gap. However,

Becker has reported discrepancies between E_a from Arrhenius plots and the S_1-T_2 energy gap determined from flash photolysis.[15] The discrepancies could result simply because the triplet vibrational level measured in triplet-triplet absorption is different from the triplet vibrational level involved in intersystem crossing. Nonetheless, E_a should be a rough measure of the S_1-T_x gap. In reality, the activation energy obtained by the Arrhenius plot is a measure of the barrier to intersystem crossing. If crossing occurs to the 0th vibrational level of T_x, E_a is truly a measure of the S_1-T_x gap. On the other hand, if crossing occurs to an upper vibrational level of T_x, the use of E_a as a measure of the energy gap is less reliable. If we assume that, for a given ester, intersystem crossing occurs to some constant vibrational level of T_x, although perhaps not the 0th vibrational level, then the trend predicted by our model of increasing E_a with decreasing S_1 energy remains valid although E_a may not be an absolute measure of the S_1-T_x gap.

Using the assumption that intersystem crossing occurs to the 0th vibrational level of the accepting triplet, the sum of the S_1 energy and E_a should give a measure of the T_x energy. Since triplet states are relatively insensitive to solvent, the sum (S_1+E_a) should be less dependent on solvent than either S_1 or E_a. If intersystem crossing occurs to a constant vibrational level of T_x other than the

0th, the sum $(S_1 + E_a)$ would still be expected to show less variability with solvent than either S_1 or E_a, even though E_a is no longer a good measure of the S_1-T_x gap. Table 5 contains the mean wavenumber, activation energy, and $(\bar{\nu}_f + E_a)$ sum for each ester/solvent pair. The error in the mean wavenumber was calculated as the frequency range corresponding to the uncertainty in wavelength around the wavelength to which frequencies were normalized $(450 \pm 1$ nm).

Returning to our experimental results, the appropriateness of our simple model will first be tested using methyl-1-anthroate. Looking at Table 3 and Figures 4,6, and 8, all three major premises of the model are substantiated by the behavior of 1-COOME in aprotic, nonaromatic solvents. Figures 4 and 6 show a linear increase in both quantum yield and activation energy with a lowering of S_1 energy. The extreme linearity (correlation coefficient=.999) for the plot of ϕ_f versus E_a (Figure 8) for 1-COOME supports the premise that these two quantities are correlated.

A plot of both $\bar{\nu}_f$ and $(\bar{\nu}_f + E_a)$ versus E_a for 1-COOME is shown in Figure 9. This shows the variation in S_1 and $(S_1 + E_a)$ for the solvents used in this study. Note that the sum $(S_1 + E_a)$ shows a more restricted range of values than S_1 alone. This lends support to our prediction that intersystem crossing terminates at a constant vibrational level of the accepting triplet and that the solvent dependence of the

Table 5

Mean Wavenumbers of Fluorescence, Activation Energies, and the Sum ($\overline{\nu}_f + E_a$) for the Ester/Solvent Pairs

Compound/ Solvent	$\overline{\nu}_f * 10^4$ cm^{-1}	E_a cm^{-1}	$(\overline{\nu}_f + E_a) * 10^4$ cm^{-1}
Methyl-1-anthroate			
cyclohexane	2.31±.01	770±14	2.39±.01
butyl acetate	2.24±.01	1215±21	2.36±.01
tetrahydrofuran	2.22±.01	1320±35	2.35±.01
acetonitrile	2.17±.01	1810±42	2.35±.01
Methyl-2-anthroate			
hexane	2.39±.01	959±28	2.48±.01
cyclohexane	2.38±.01	1236±60	2.50±.02
Methyl-9-anthroate			
cyclohexane	2.23±.01	935±21	2.32±.01
butyl acetate	2.19±.01	1061±35	2.30±.01
ethyl acetate	2.18±.01	1348±119	2.31±.02
acetonitrile	2.15±.01	1439±21	2.29±.01
dimethyl formamide	2.14±.01	1586±42	2.30±.01
dimethyl sulfoxide	2.12±.01	1393±14	2.26±.01

Figure 9

$$\bar{\nu}_f \text{ and } (\bar{\nu}_f + E_a) \text{ versus } E_a \text{ for 1-COOME}$$

For 1-COOME, the sum $(S_1 + E_a)$ shows a more restricted range of values than S_1 alone. This lends some support to our prediction that intersystem crossing terminates at a constant vibrational level of the accepting triplet and that the solvent dependence of the triplet level is less than that of S_1.

Solvent Key

C - cyclohexane
A - acetonitrile
BA - butyl acetate
THF - tetrahydrofuran
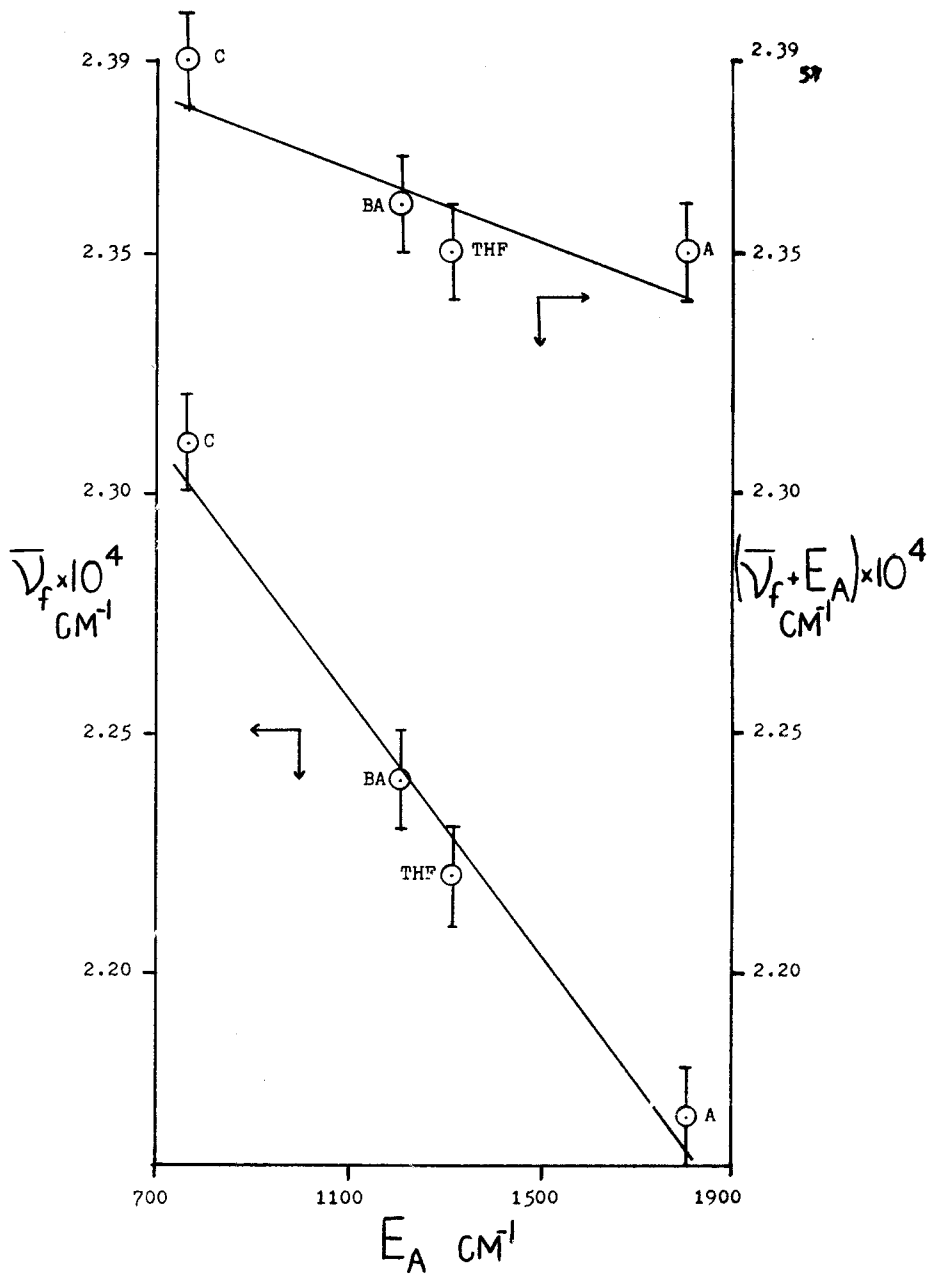
triplet level is less than that of S_1.

Although fewer results are available than for 1-COOME, the fluorescence behavior of 2-COOME in aprotic,nonaromatic solvents is also quite well predicted by the simple model. In Figure 4, the quantum yield was found to increase with decreasing S_1 energy up to tetrahydrofuran. Once again, the limited number of activation energies for 2-COOME restrict statements about general trends between E_a and S_1 or ϕ_f and E_a. However, the fact that the two available activation energies do increase with decreasing S_1 energy supports the second premise of the model. Additionally, the validity of a correlation between ϕ_f and E_a is reinforced when the data for 2-COOME is added to that for 1-COOME. The correlation coefficient for the combined data (.986) reflects a high degree of linearity for the relation between ϕ_f and E_a (Figure 8).

In contrast to the first premise of our model, the ϕ_f of 2-COOME was found to decrease in going from tetrahydrofuran to dimethyl formamide, the solvent in which 2-COOME has the lowest S_1 energy. From our model, we expect the ϕ_f to increase to and remain at unity as S_1 energy continues to decrease. We may speculate that internal conversion or intersystem crossing to a triplet level lower than T_x may become competitive with fluorescence for 2-COOME in dimethyl formamide. Alternately, a specific solvent induced lowering

of T_x may allow intersystem crossing to again become effi-
cient in deactivating S_1 by decreasing the S_1-T_x gap.

Since only two data points are available for 2-COOME
in Table 5, little can be said about the relative solvent
dependence of the sum $(S_1 + E_a)$ in comparison to that of S_1
alone. However, going back to Table 3, we note a steep in-
crease in the quantum yield for 2-COOME with a relatively
small decrease in S_1 energy. This implies that the effi-
ciency of intersystem crossing is greatly reduced by small
increases in the S_1-T_x energy gap due to the lowering of S_1.

Turning our attention to methyl-9-anthroate, we recall
that the experimental data show some behavior in contrast
to that of 1 and 2-COOME. In Figure 5, 9-COOME exhibits a
general decrease in quantum yield with decreasing S_1 energy,
although scatter exists. Nevertheless, the trend of in-
creasing activation energy with decreasing S_1 energy observed
for both 1 and 2-COOME is also seen for 9-COOME in Figure 7.
In the plot of $\emptyset_f$ versus E_a (Figure 8), the data for 9-COOME
show no highly linear relationship as seen with the other
two methyl esters. It should be noted that data points for
two protic, nonaromatic solvents, isopropanol and ethanol,
are included in the plot. If anything, 9-COOME shows a
general trend which is opposite to that of 1 and 2-COOME;
that is, $\emptyset_f$ decreases rather than increases with increasing
E_a. Also, it is interesting to note in Figure 8, with the

exception of two nonpolar solvents, cyclohexane and butyl acetate, that all of the activation energies fall within a one kcal/mole range from 3.67-4.67. In other words, a small change in E_a accompanies a relatively large change in ϕ_f.

The solvent dependence of S_1 and $(S_1 + E_a)$ versus E_a for 9-COOME are shown in Figure 10. Note that if we ignore the dimethyl sulfoxide points, the data agree quite well with the 1-COOME plot (see Figure 9). That is, the range of $(S_1 + E_a)$ values is smaller than for S_1 alone, showing $(S_1 + E_a)$ to be relatively less dependent on solvent.

In summary, E_a does <u>increase</u> with decreasing S_1 energy for 9-COOME, as the simple model predicts. However, the fact that the ϕ_f shows a general <u>decrease</u> with decreasing S_1 energy means that an inverse correlation exists between ϕ_f and E_a for 9-COOME. That is , of course, opposite to that predicted by the simple model and to the behavior actually seen for 1 and 2-COOME where ϕ_f and E_a are <u>directly</u> related.

Speculation allows us to present some possible reasons for the anomalous behavior of 9-COOME. Activation energy values may be a reliable measure of the $S_1 - T_x$ split, but some other factor may actually control the rate of intersystem crossing in 9-COOME. Indeed, the sum of $(S_1 + E_a)$ for 9-COOME, just as for 1-COOME, is less dependent on E_a than is S_1, the only exception being the dimethyl sulfoxide points which are quite low for both S_1 and $(S_1 + E_a)$ indicat-

Figure 10

$\bar{\nu}_f$ and $(\bar{\nu}_f + E_a)$ versus E_a for 9-COOME

If we ignore the dimethyl sulfoxide points, the 9-COOME data agree quite well with the 1-COOME data. That is, the variation in $(S_1 + E_a)$ values is smaller than for S_1, showing $(S_1 + E_a)$ to be relatively less dependent on solvent.

Solvent Key

C - cyclohexane
BA - butyl acetate
EA - ethyl acetate
A - acetonitrile
DMF - dimethyl formamide
DMSO - dimethyl sulfoxide
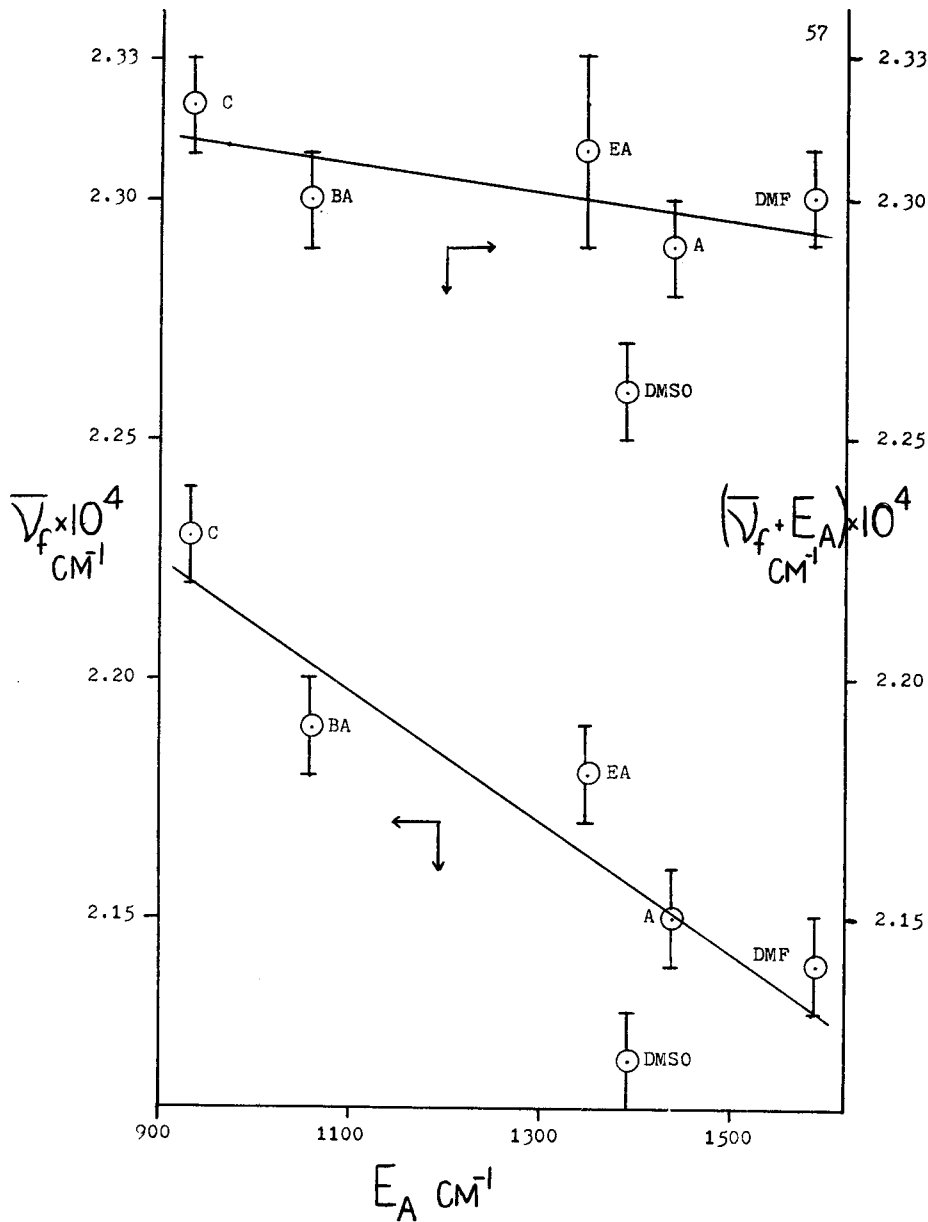
ing specific solvation effects or possibly water contamination of the dimethyl sulfoxide. The relative insensitivity of $(S_1 + E_a)$ as a measure of T_x supports the assumption that intersystem crossing occurs to a constant vibrational level of T_x in 1 and 9-COOME, and therefore, E_a may be a good measure of the $S_1 - T_x$ gap.

The observed linear relationship expressed by the Arrhenius equation may be fortuitous for 9-COOME, and such an assumption for the excited state behavior may be unwarranted. In this case, E_a values could be given no physical interpretation. Labhart has shown cases where there are portions of Arrhenius plots corresponding to relatively large ranges of temperature where within experimental errors an approximation by a straight line is satisfactory.[22] However, over the total temperature range of such plots, substantial curvature is noted and therefore it is impossible to relate E_a to a known physical process like intersystem crossing. Indeed, the linearity of our Arrhenius plots may lead us to the conclusion that the relatively small temperature range used in this work $(40-50^{\circ}C)$ is suspect. The limitations of our temperature range might show up in Arrhenius plots from an expanded temperature range $(200^{\circ}C)$.

We should also remember the considerable geometry change in 9-COOME upon excitation. Differences in the shape of the three molecules in the excited state should be pointed out.

Perhaps the equilibrium geometry of the excited state is solvent dependent, affecting the shape of the excited state potential energy surface. Changes in the shape of the potential energy surface would, in turn, affect the extent of state mixing and overlap between S_1 and upper triplet excited states which are responsible for promoting intersystem crossing.

In conclusion, despite the possible limitations on the use of the Arrhenius expression and our simple model, the observed solvent dependence of the fluorescence quantum yield of methyl-1-anthroate can be fit by our simple model very well. In addition, the premises of the simple model break down only slightly when applied to methyl-2-anthroate. Clearly, methyl-9-anthroate is a unique molecule whose fluorescence behavior can not be interpreted by the constraints imposed by our simple model.

APPENDICES

APPENDIX I.

Explanation of the Least Squares Analysis Computer Program:

This program was written to accept the fluorescence versus temperature data for the anthroate esters in different solvents and fit the data to the Arrhenius expression. In addition, the data ($\log(\phi_f^{-1}-1)$ vs. $1/T$) is graphed using the subroutine PLOTG on file in the computer.

Variable Listing: The variables used and their explanation as they appear in the program are as follows:

Variable name	Explanation
NTRIAL	Number of temperature work trials
TITLE	Alphanumeric string of 80 characters identifying trial compound, solvent, sample number, run number, and date
N	Number of data points in trial
RTN	Room temperature refractive index of solvent
DNDT	Change in refractive index per degree centigrade temperature change
RT	Room temperature in degrees centigrade
PHIRT	Room temperature quantum yield
TEMP(NN)	Centigrade temperature
PKHT(NN)	Peak height (fluorescence intensity maximum) for the fluorescence band in millimeters from spectral baseline
ABSCOR(NN)	Absorbance correction factor for temperature ($Abs(23)/Abs(T)$)
NT	Refractive index at TEMP(NN)

Variable name	Explanation
PHI(NN)	Quantum yield at TEMP(NN)
X(NN) Y(NN)	Independent and dependent variables to be fit
SLOPE	Slope of the fit
INTCPT	Intercept of the fit
EACT	Activation energy in kcal/mole
R	Correlation coefficient

Flowchart :

```
( Start ) → [Read NTRIAL] → <Do 20 J=1,NTRIAL> → | X1=0
                                                   | X2=0
                                                   | Y1=0  → [Read TITLE]
                                                   | Y2=0
                                                   | XY=0

[Read TEMP(NN), PKHT(NN), ABSCOR(NN)] ← <Do 60 NN=1,N> ← [Write headings] ← [Read N, RTN,DNDT, RT,PHIRT] ← [Write TITLE]

(A)
(B)  PHI(NN)=PHIRT*(NT**2)*PKHT(NN)*ABSCOR(NN)
              (RTN**2)*PKHT(1)
     X(NN)=(1/TEMP(NN)+273.)*1000.
     Y(NN)=ALOG(1/PHI(NN)-1.)

yes ←  <? NN=N> → | X1=X1+X(NN)
         no       | X2=X2+X(NN)**2      → [Write TEMP(NN),
                  | Y1=Y1+Y(NN)            PKHT(NN),PHI(NN),
                  | Y2=Y2+Y(NN)**2         X(NN),Y(NN)]
                  | XY=XY+X(NN)*Y(NN)

| SXX=X2-X1**2/N    | SLOPE=SXY/SXX                → [Write
| SXY=XY-X1*Y1/N    | INTCPT=Y1/N-SLOPE*X1/N          SLOPE,
| SYY=Y2-Y1**2/N    | EACT=-SLOPE*2.303*1.987         INTCPT]

(D) (C) → [Write R] ← [R=SLOPE*(SXX/SYY)**.5] ← [Write EACT]

no ← <? J=NTRIAL> → yes → ( END )          (C) → [PLOTG] → (D)

(A) → [NT=RTN+DNDT*(TEMP(NN)-RT)] → (B)
```

Program Listing:

```
$RESET FREE
$SET AUTOBIND
$BIND = FROM CUBE/= ON ACADEMIC
FILE  5(KIND=DISK,TITLE="PLOT",MAXRECSIZE=14,BLOCKSIZE=420)
      DIMENSION PC(14),XID(6),YID(6),HEAD(21)
      DATA HEAD/"LOG1/"," PHI-1)"," VERSU","S 1/TE","MP*100",
     *"O       ",15*"        "/
      DATA XID/"1/TEMP","*1000 ",4*"      "/
      DATA YID/"LOG(1/","PHI-1)",4*"      "/
      PC(13)=5
C     TEMP=CENTIGRADE TEMPERATURE
C     PKHT=PEAK HEIGHT IN MM.
C     ABCCOR=ABSORBANCE CORRECTION FACTOR FOR TEMPERATURE
C     TITLE=COMPOUND,SOLVENT,SAMPLE,RUN,DATE
C     PHI=QUANTUM YIELD
      DIMENSION TITLE(20),TEMP(20),PKHT(20),PHI(20),X(20),
     *Y(20),ABSCOR(20)
      REAL NT,INTCPT
      READ(5,10) NTRIAL
C     NTRIAL=NUMBER OF TRIALS
10    FORMAT(I3)
      DO 20 J=1,NTRIAL
      X1=0
      X2=0
      Y1=0
      Y2=0
      XY=0
      READ(5,30) (TITLE(I),I=1,20)
30    FORMAT(20A4)
      WRITE(6,40) (TITLE(I),I=1,20)
40    FORMAT(1H1,20A4,//)
      READ(5,50) N,RTN,DNDT,RT,PHIRT
C     N=NUMBER OF DATA POINTS
C     RTN=ROOM TEMPERATURE REFRACTIVE INDEX
C     DNDT=CHANGE IN REFRACTIVE INDEX/CHANGE IN TEMPERATURE
C     RT=ROOM TEMPERATURE
C     PHIRT=ROOM TEMPERATURE QUANTUM YIELD
50    FORMAT(I3,4F10.2)
      PC(1)=N
      WRITE(6,55)
55    FORMAT(62HO   TEMP      PEAK HT.    PHI    (1/TEMP*
     *1000)   LOG(1/PHI-1))
      DO 60 NN=1,N
      READ(5,70) TEMP(NN),PKHT(NN),ABSCOR(NN)
70    FORMAT(3F10.2)
      CALL INDEX(RTN,DNDT,RT,TEMP(NN),NT)
C     NT=REFRACTIVE INDEX AT TEMP(NN)
      PHI(NN)=(PHIRT*(NT**2)*PKHT(NN)*ABSCOR(NN))/((RTN**2)
```

```
        **PKHT(1))
         X(NN)=(1/(TEMP(NN)+273.))*1000.
         Y(NN)=ALOG10((1/PHI(NN))-1)
  80     WRITE(6,80) TEMP(NN),PKHT(NN),PHI(NN),X(NN),Y(NN)
         FORMAT(1HO,F9.1,F11.1,F11.3,F11.3,F16.3)
         X1=X1+X(NN)
         X2=X2+X(NN)**2
         Y1=Y1+Y(NN)
         Y2=Y2+Y(NN)**2
         XY=XY+X(NN)*Y(NN)
  60     CONTINUE
         SXX=X2-X1**2/N
         SXY=XY-X1*Y1/N
         SYY=Y2-Y1**2/N
         SLOPE=SXY/SXX
  C      SLOPE=SLOPE
         INTCPT=Y1/N-SLOPE*X1/N
  C      INTCPT=INTERCEPT
         EACT=-SLOPE*2.303*1.987
  C      EACT=ACTIVATION ENERGY
  90     WRITE(6,90) SLOPE,INTCPT
         FORMAT(11HOTHE FIT IS,F7.3,4H X +,F8.3)
  100    WRITE(6,100) EACT
         FORMAT(21HOACTIVATION ENERGY = ,F7.2)
         R=SLOPE*((SXX/SYY)**.5)
  C      R=CORRELATION COEFFICIENT
  110    WRITE(6,110) R
         FORMAT(27HOCORRELATION COEFFICIENT = ,F7.4)
  20     CALL PLOTG(X,Y,PC,XID,YID,HEAD)
         CONTINUE
         STOP
         END
         SUBROUTINE INDEX(RTN,DNDT,RT,TEMP,NT)
         REAL NT
         NT=RTN+DNDT*(TEMP-RT)
         RETURN
         END
```

Data Input: In making a data file for this program,
the line sequence is as follows:

Line 1- Enter the number of fluorescence versus temperature
        trials to be fit (FORMAT(I3))

Line 2- Enter the compound, solvent, sample number, run
        number, and date for the first trial (FORMAT(20A4))

Line 3- Enter the number of data points (N), room temperature
        refractive index (RTN), refractive index change with
        temperature (DNDT), room temperature (RT), and the
        room temperature quantum yield (PHIRT) for the
        first trial (FORMAT(I3,4F10.2))

Line 4- Enter data for the room temperature reading in the
        first trial-
        a) temperature
        b) peak height (fluorescence intensity maximum)
           measured in millimeters from the spectral base-
           line
        c) absorbance correction factor for the temperature
        (FORMAT(3F10.2))
        *The data for the room temperature measurement must
        be the first entered.

Line 5,6,7...- Enter the remaining data sets for the trial,
        one per line, following the format of Line 4.

If more than one fluorescence versus temperature trial is
to be fit, repeat the data input for each trial as explained
for trial one beginning at Line 2.

If the fluorescence versus temperature work was recorded
while exciting at a valley in the absorption spectrum,
absorbance versus temperature correction values are not
necessary. Therefore, a value of 1. should be entered for
the absorption correction value at each temperature in the
trial.

APPENDIX II.

Explanation of the Fluorescence Mean Wavenumber Computer Program:

This program accepts data from uncorrected fluorescence spectra from 380-600 nm and calculates the corrected mean wavenumber of fluorescence as a measure of the S_1 energy. The mean wavenumber ($\bar{\nu}_m$) is calculated from the following relation:[2]

$$\int_{\bar{\nu}_1}^{\bar{\nu}_m} F(\bar{\nu})d\bar{\nu} = \tfrac{1}{2}\int_{\bar{\nu}_1}^{\bar{\nu}_2} F(\bar{\nu})d\bar{\nu}$$

where $\bar{\nu}_1$ and $\bar{\nu}_2$ are the minimum and maximum wavenumbers at which measurable fluorescence occurs. $F(\bar{\nu})$ is the corrected fluorescence intensity at a given wavenumber. The uncorrected spectra are corrected for instrument sensitivity and then converted to a wavenumber scale. To obtain $\bar{\nu}_m$, the area under the curve from $\bar{\nu}_1$ to $\bar{\nu}_m$ is compared with the total area under the spectrum. The mean wavenumber is used as a measure of the S_1 energy so that spectra with different degrees of structure may be compared.

Variable Listing: The variables used in the program with their explanation are as follows:

Variable name | Explanation

SEN(I) | Sensitivity correction factors for the MPF-2A for each 2 nm from 380-600 nm

FREQ(I) | Frequency conversion factor data ($d\lambda/d\bar{\nu}$) normalizing intensities to the frequency at 450 nm

Variable name	Explanation
TITLE	Alphanumeric string identifying the ester and solvent
NDATA	Number of wavelength data points for the run
FOW(I)	Uncorrected fluorescence intensity as a function of wavelength
FTW(J)	Corrected fluorescence intensity as a function of wavelength
FTF(J)	Corrected fluorescence intensity as a function of frequency
DFREQ	Frequency interval between adjacent FTF values divided by 10
SUM	Summation of the area beneath the corrected fluorescence curve as a function of frequency
AREA	One-half the area under the corrected fluorescence frequency curve
WAVNUM	Mean wavenumber of fluorescence

Flowchart:

```
( Start ) → [ AREA=9999999999. ] → / Read
                                      SEN(I),I=1,111
                                      FREQ(I),I=1,111 /

/ Read                Read          Read
  FOW(I),     ←       NDATA   ←     TITLE
  I=1,NDATA /

⬡ Do 40        ← [ Z=0. ]
  J=1,NDATA

[ FTW(J)=FOW(J)/SEN(J)        ◇ Z<1.  →no→  [ DFREQ=(FTF(J)-
  PTF(J)=FTW(J)*FREQ(J)              |              FTF(JJ))/10. ]
  JJ=J-1 ]                          yes

◇ ?        no    ◇ SUM      [ SUM=SUM+((K*DFREQ)    ⬡ Do 50
  K=10    →→→→→    ≥    ←      +FTF(JJ)) ]     ←      K=1,10
  |yes            AREA
  no              |yes

◇ ?        yes   [ AREA=SUM/2.       [ WAVNUM=1000/(JJ*2+K*.2+378) ]
  J=NDATA  →→→     SUM=0. ]
  |
  no                                  / Write
                                        TITLE /
[ SUM=SUM+PTF(J)
  Z=Z+1 ]                             / Write
                                        WAVNUM /

                                      ( End )
```
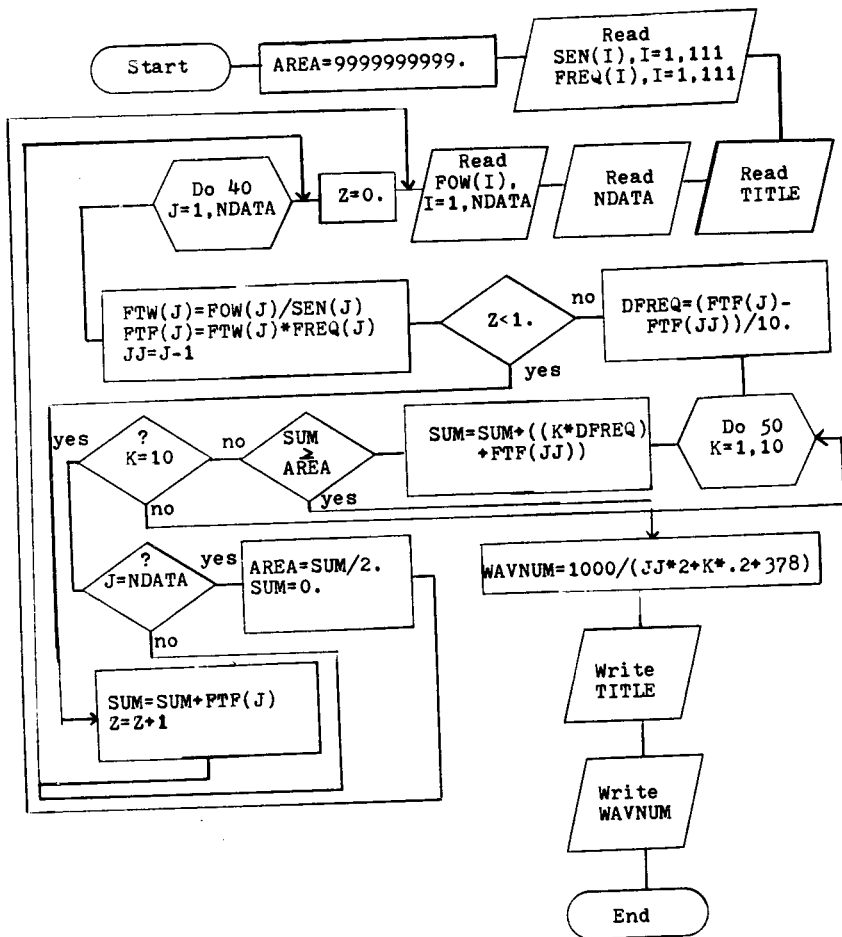
Program Listing:

```
     DIMENSION SEN(125),TITLE(20),FOW(125),FTW(125),FTF(125),
    *FREQ(125)
     AREA=9999999999.
     READ(5,10) (SEN(I),I=1,111)
     READ(5,10) (FREQ(I),I=1,111)
10   FORMAT(8F10.0)
     READ(5,20) (TITLE(I),I=1,20)
20   FORMAT(20A4)
     READ(5,30) NDATA
30   FORMAT(I3)
     READ(5,10) (FOW(I),I=1,NDATA)
35   Z=0.
     DO 40 J=1,NDATA
     FTW(J)=FOW(J)/SEN(J)
     FTF(J)=FTW(J)*FREQ(J)
     JJ=J-1
     IF(Z.LT.1) GO TO 60
     DFREQ=(FTF(J)-FTF(JJ))/10.
     DO 50 K=1,10
     SUM=SUM+((K*DFREQ)+FTF(JJ))
     IF(SUM.GE.AREA) GO TO 70
50   CONTINUE
     GO TO 40
60   SUM=SUM+FTF(J)
     Z=Z+1
40   CONTINUE
     AREA=SUM/2.
     SUM=0.
     GO TO 35
70   WAVNUM=1000./(JJ*2.+K*.2+378.)
     WRITE(6,80) (TITLE(I),I=1,20)
80   FORMAT(1H0,20A4,/)
     WRITE(6,90) WAVNUM
90   FORMAT(1H0,"MEAN WAVENUMBER OF FLUORESCENCE=",F5.2,
    *"*10+4 CM-1")
     STOP
     END
```

<u>Data Input:</u> The line sequence for the data file for this program is as follows:

Lines 1-14- Sensitivity correction factors for the MPF-2A for every 2 nm over the range 380-600 nm (FORMAT(8F10.0))

Lines 15-28- Frequency conversion factor data ($d\lambda/d\bar{\nu}$) for every 2 nm over the range 380-600 nm (FORMAT(8F10.0))

Line 29- Enter compound and solvent (TITLE) (FORMAT(20A4))

Line 30- Enter the number of data points (NDATA), or peak heights, for the run (FORMAT(I3))

Line 31,32...- Enter peak heights (uncorrected fluorescence intensities in millimeters from the spectral baseline) for every 2 nm starting at 380 nm and continuing to the longest wavelength in the spectrum having a nonzero intensity (FORMAT(8F10.0))

Lines 1-28 are used for every ester/solvent pair. Therefore, for each new ester/solvent pair, only lines numbered from 29 to the end of the data file must be changed before rerunning the program for the new ester/solvent pair.

REFERENCES

1. J. Trotter, Acta Crystalogr., $\underline{13}$, 732 (1962); as referred to in T.C. Werner, Thomas Matthews, and Babs Soller, J. Phys. Chem., $\underline{80}$, 533 (1976).

2. T.C. Werner, Thomas Matthews, and Babs Soller, J. Phys. Chem., $\underline{80}$, 533 (1976).

3. T.C. Werner and D.M. Hercules, unpublished studies; as referred to in T.C. Werner, Thomas Matthews, and Babs Soller, J. Phys. Chem., $\underline{80}$, 533 (1976).

4. Y. Lui and S.P. McGlynn, J. Mol. Spectrosc., $\underline{49}$, 214 (1974); as referred to in T.C. Werner, Thomas Matthews and Babs Soller, J. Phys. Chem., $\underline{80}$, 533 (1976).

5. R.O.C. Norman and P.D. Ralph, J. Chem. Soc., 2221 (1961); as referred to in T.C. Werner, Thomas Matthews, and Babs Soller, J. Phys. Chem., $\underline{80}$, 533 (1976).

6. William Hawkins, Undergraduate Thesis, Chem. Dept., Union College, 1976.

7. John Facci, Undergraduate Thesis, Chem. Dept, Union College, 1977.

8. Synthesized by T.C. Werner at Union College.

9. Thomas Matthews, Undergraduate Thesis, Chem. Dept., Union College, 1975.

10. T.C. Werner and Ronald Hoffman, J. Phys. Chem., $\underline{77}$, 1611 (1973).

11. R.F. Chen, Anal. Biochem., $\underline{20}$, 339 (1967).

12. T.C. Werner, Revised Procedure for $\emptyset_f$ Determinations (7/24/79).

13. J.A. Riddick and W.B. Bunger, "Techniques of Chemistry Vol. II, Organic Solvents", Wiley-Interscience, New York, 1970.

14. E. Kosower, "An Introduction to Physical Organic Chemistry", John Wiley and Sons, New York, 1968, page 305.

15. Ralph S. Becker, "Theory and Interpretation of Fl cence and Phosphorescence", Wiley Interscience, Ne

York, N.Y., 1969, chapter 11.

16. E. Vander Donckt and G. Porter, Trans. Faraday Soc., 64, 3218 (1968); as referred to in T.C. Werner and Ronald Hoffman, J. Phys. Chem., 77, 1611 (1973).

17. Kam-Chu Wu and William R. Ware, J. Am. Chem. Soc., 101, 5906 (1979).

18. W.R. Ware and B.A. Baldwin, J. Chem. Phys., 43, 1194 (1965).

19. R.G. Bennett and P.J. McCartin, J. Chem. Phys., 44, 1969 (1966).

20. T. Medinger and F. Wilkinson, Trans. Faraday Soc., 61, 620 (1965); as referred to in T.C. Werner, William Hawkins, John Facci, Russell Torrisi, and Terry Trembath, J. Phys. Chem., 82, 298 (1978).

21. J. Laposa, E. Lim, and R. Kellogg, J. Chem. Phys., 42, 3025 (1965); as referred to in T.C. Werner, William Hawkins, John Facci, Russell Torrisi, and Terry Trembath, J. Phys. Chem., 82, 298 (1978).

22. H. Labhart, Chem. Phys. Lett., 1, 263 (1967).